HHS Public Access

Author manuscript

IEEE Trans Biomed Eng. Author manuscript; available in PMC 2021 March 01.

Published in final edited form as:

IEEE Trans Biomed Eng. 2020 March ; 67(3): 876–882. doi:10.1109/TBME.2019.2922879.

Wireless Resonant Circuits Printed Using Aerosol Jet Deposition for MRI Catheter Tracking

Caroline D. Jordan,
Department of Radiology and Biomedical Imaging at the University of California San Francisco, San Francisco, CA, USA.

Bradford R. H. Thorne,
Department of Radiology and Biomedical Imaging, University of California San Francisco, San Francisco, CA, USA, and is now with Purdue University, West Lafayette, IN, USA.

Arjun Wadhwa,
Quest Integrated, LLC, Kent, WA, USA and is now with École de technologie supérieure, Montreal, QC, CA.

Aaron D. Losey,
Department of Radiology and Biomedical Imaging at the University of California San Francisco, San Francisco, CA, USA.

Eugene Ozhinsky,
Department of Radiology and Biomedical Imaging at the University of California San Francisco, San Francisco, CA, USA.

Sravani Kondapavulur,
Department of Radiology and Biomedical Imaging at the University of California San Francisco, San Francisco, CA, USA.

Vincent Fratello,
Quest Integrated, LLC, Kent, WA, USA.

Teri Moore,
Department of Radiology and Biomedical Imaging at the University of California San Francisco, San Francisco, CA, USA.

Carol Stillson,
Department of Radiology and Biomedical Imaging at the University of California San Francisco, San Francisco, CA, USA.

Colin Yee,
Department of Radiology and Biomedical Imaging at the University of California San Francisco, San Francisco, CA, USA.

Ronald D. Watkins,
Department of Radiology at Stanford University, Stanford, CA, USA.

corresponding author. steven.hetts@ucsf.edu.

Greig C. Scott,
Department of Electrical Engineering at Stanford University, Stanford, CA, USA.

Alastair J. Martin,
Department of Radiology and Biomedical Imaging at the University of California San Francisco, San Francisco, CA, USA.

Xiaoliang Zhang [Member, IEEE],
Department of Radiology and Biomedical Imaging, University of California, San Francisco, San Francisco, CA, USA, and is now with the Department of Biomedical Engineering at the University of Buffalo, The State University of New York, Buffalo, NY, USA.

Mark W. Wilson,
Department of Radiology and Biomedical Imaging at the University of California San Francisco, San Francisco, CA, USA.

Steven W. Hetts
Department of Radiology and Biomedical Imaging at the University of California San Francisco, San Francisco, CA, USA

Abstract

Interventional magnetic resonance imaging could allow for diagnosis and immediate treatment of ischemic stroke; however, such endovascular catheter-based procedures under MRI guidance are inherently difficult. One major challenge is tracking the tip of the catheter, as standard fabrication methods for building inductively coupled coil markers are rigid and bulky. Here, we report a new approach that uses aerosol jet deposition to 3D print an inductively coupled RF coil marker on a polymer catheter. Our approach enables lightweight, conforming markers on polymer catheters and these low-profile markers allow the catheter to be more safely navigated in small caliber vessels. Prototype markers with an inductor with the geometry of a double helix are incorporated on catheters for *in vitro* studies, and we show that these markers exhibit good signal amplification. We report temperature measurements, and finally demonstrate feasibility in a preliminary *in vivo* experiment. We provide material properties and electromagnetic simulation performance analysis. This work presents fully aerosol jet-deposited and functional wireless resonant markers on polymer catheters for use in 3T clinical scanners.

Index Terms

wireless resonant circuits; interventional MRI; aerosol jet deposition; tracking markers; double helix design

I. Introduction

STROKE is a leading cause of long-term disability and the fifth leading cause of death, with approximately 690,000 people suffering from an acute ischemic stroke each year in the United States [1]. While catheter-based endovascular embolectomy under real-time X-ray angiographic guidance is an effective treatment for patients suffering a large vessel occlusion acute ischemic stroke, about 10% or fewer of potentially eligible patients receive

such treatments [2]. This is in part due to the narrow recommended time window for therapy within 3–6 hours of stroke onset; however, there is a growing paradigm shift that stroke treatment could potentially follow an expanded time window, if brain tissue viability was known [3]. Recent clinical trials based on perfusion imaging are now allowing stroke patients with viable tissue to be treated up to 24 hours after the onset of symptoms in some cases [4], [5]. Interventional magnetic resonance imaging (MRI) could allow for accurate diagnosis and immediate treatment, since diffusion weighted imaging in combination with perfusion imaging is the gold standard in determining if brain tissue is still viable. However, the magnetic fields in the MRI scanner create a challenging environment for the standard guidewires and catheters used for clot removal, which contain metal components to achieve optimal mechanical properties. During an MRI scan, long conductive structures can give rise to large electric fields at the tip of the device, which can cause unsafe tissue heating [6]. Furthermore, tracking markers are needed to localize the tip of the catheter and must have both a low side profile and be flexible enough to navigate safely in small vessels. If there was a marker that allowed for reliable, safe, and straightforward tracking and visualization of endovascular catheters, this could overcome one of the barriers to clinical adoption by interventional radiologists to use MRI in combination with embolectomy treatment [7].

A. Tracking Markers

Methods for MRI markers have been broadly categorized in the interventional MRI literature as passive or active, or as a hybrid technique, sometimes referred to as semi-active. Passive approaches display the catheter in the image, often using signal void or differences in magnetic susceptibility between the catheter and surroundings, causing local B_0 field inhomogeneities [8]. Active approaches typically use a micro-coil at the tip of catheter, and have wires running down the length of the catheter to receive information about the location of the catheter tip [8]. The hybrid technique has referred to resonant markers, implemented as an inductively coupled coil, or more specifically, a circuit with a capacitor (C) connected to a coil, which has inductance (L) and intrinsic resistance (R). This RLC circuit can be built on the tip of the catheter to provide local signal amplification of the B_1+ field [9]. The circuit inductively couples with the magnetic flux from the radiofrequency (RF) pulse, resulting in induced current in the circuit, and the production of a local magnetic field [10]. The locally amplified B_1+ field produces higher flip angles in the surrounding region, which in turn can enhance signal or alter contrast in MR images. One of the earliest implementations of an inductively coupled coil marker used a solenoid inductor coil geometry surrounding a small solution, which was used as a fiducial marker for localization [9].

Such wireless resonant circuits [11], or inductively coupled RF coils [12], have previously been built on top of large diameter guide catheters using a variety of fabrication methods and geometries. More recently, wireless resonant circuits have been built on catheters for interventional MRI applications, using inductor coil geometries such as a rectangular surface loop coil [13], two opposing solenoids oriented at 45° relative to the axis of the catheter [14], and flat spiral coils [15]. Recent work proposed an inductor geometry of a double helix, each arm tilted 45° with respect to the z-axis [16], [17].

Often, these resonant markers have been built by hand using discrete elements, which introduces a number of challenges, including reproducibility, flexibility, and increased profile thickness of the catheter. In particular, the increased size and decreased flexibility of such a circuit at the catheter tip makes it impractical for neurointerventional use. A number of microfabrication methods for building markers on catheters have been explored beyond manual wire winding, including flexible printed circuit boards, hot embossing, thin-film techniques, and aerosol deposition processes [10]. While thin-film technology can deposit micrometer scale features, it requires a significant investment for each new application, and is a 2-dimensional process, traditionally requiring a rigid, planar framework, and is not ideal for manufacturing 3-dimensional (3D) conformal electronics, such as those required for catheters [15]. Aerosol jet deposition, a new additive manufacturing process, is ideal for building micrometer size electronics, is CAD-file driven [18], and can print conformal electronics on various surfaces. We use aerosol jet deposition to print a complete, distributed LC circuit, using the double helix inductor geometry on a polymer catheter for interventional MRI use at 3.0T.

The wireless resonant circuit can be modeled as an LC circuit, where the inductor is connected in parallel to the capacitor [19]. A current is induced in the circuit, due to inductive coupling with both the RF transmit coil and the local MR signal in the immediate vicinity. This generates an associated magnetic field and flux, enhancing the local B_1. There is local amplification of the flip angle achieved during transmit, and then enhanced local sensitivity during receive. During receive, the marker is loosely coupled to the receive coil, so the B_1 of each combine to enhance the local sensitivity at the marker. The coupling is also dependent on the orientation of the marker with respect to the MR signal phase [19]. The magnetic flux through a surface is calculated by the inner product of the surface normal vector and the magnetic field. Given the double helix design, the surface normal vector cannot be uniquely defined for the whole coil as a single analytical quantity. The current in the inductor is amplified depending on the quality factor, Q, of the resonant circuit. A long capacitor with parallel plates running side-by-side can be effectively modeled as a twin-lead transmission line, which has a distributed capacitance and inductance.

II. Methods

A. Catheter fabrication

Polymer catheters were constructed in a catheter fabrication facility (Penumbra, Alameda, CA). The catheters consisted of a polytetrafluoroethylene (PTFE) catheter substrate, braided with polyether ether ketone (PEEK) fibers, and sealed with a thermoplastic elastomer, polyether block amide (Pebax 72D, Zeus Inc. Orangeburg, SC). The polymer catheter had an outer diameter of approximately 2.248 mm (Table I).

B. Resonant marker microfabrication

All conductive prints used a water-based silver nanoparticle flake ink (NovaCentrix HPS-108AE1, NovaCentrix, Austin, TX) and the dielectric ink was polyimide ink (ε_r = 3.6–3.7) (Sigma Aldrich, St. Louis, MO), with the material properties given in Table I. The double helix included 10 turns, tilted at a helix angle of 22.5°, for a 3.53 mm pitch (πr), for

a total length of 35.31 mm (10πr). The conductive traces were printed with approximately a 250 μm trace width and a 4 μm thickness. The capacitor plates were printed measuring 180 mm long, with a 280–300 μm width using an approximately 50 μm printed trace width, a 4 μm trace thickness, and 200 μm separation of the plates (Fig. 1). An aerosol jet deposition system (Aerosol Jet® 300P system, Optomec, Albuquerque, NM) was used for printing (Quest Integrated LLC, Kent, WA), with a tolerance of ±60 μm (Fig. 2a). First, the single helical arm and capacitor plates were printed with the silver ink and cured for 1 hour. Second, the dielectric ink for the capacitor and intermediate encapsulation for the first coil were printed and cured for 2 hours. The first printed coil was left exposed at the tip for electrical connection. Third, the top helical arm was printed with the silver ink and cured for 30–60 minutes. Finally, the dielectric ink, was printed to insulate the entire double helix coil and capacitor assembly, and the completed print was cured for 2 hours.

C. In vitro image acquisition

The catheter was placed in a rectangular water phantom doped with $CuSO_4$ and the phantom was oriented either parallel or perpendicular to B_0. Images were acquired in both orientations at 3.0T (Discovery MR 750w, GE Healthcare, Chicago, IL) using the body coil for transmit (B_1+) and an 8-channel cardiac receive-only coil. A balanced steady state free precession (bSSFP) sequence was acquired for visualization, and a Bloch-Siegert B_1+ map [20], [21] was acquired for flip angle quantification, using a coronal scan plane, a 10 mm slice thickness, and the imaging parameters in Table II. An ROI was manually drawn around the entire marker to measure the mean signal, and then the ratio with the nearby background water signal was calculated to measure the relative amplification factor. All image processing was performed in MATLAB 2016a (MathWorks Inc., Natick, MA).

D. Simulations

All simulations were performed using finite element method software (COMSOL 5.3a, Burlington, MA) on a 64-bit Windows 7 computer with 32.0 GB RAM, and an Intel® Xeon® CPU E5–1620 0 @ 3.60 GHz. The simulated double helix was modeled as a perfect electric conductor with no resistance, in parallel with a 14 pF capacitor, and had a radius of 2.2 mm, and a pitch distance of 3.455 mm for an angle of 22.5°. A frequency domain analysis of the electromagnetic field was performed at 130 MHz.

E. Temperature measurements

A hydroxyethyl cellulose gel was prepared [22], and four temperature probes (Luxtron, LumaSense Technologies, Inc. Santa Clara, CA) were placed in the gel. Temperature was recorded every second during a fast spin echo (FSE) sequence, as well as two minutes before and after the scan, for a total scan time of 15:02 min (Table II). The baseline temperature of each probe at room temperature was subtracted for comparison. We then acquired a set of MR thermometry images in an oblique scan plane with a 10 mm slice thickness, parallel to the catheter using a fast spoiled gradient echo sequence (FSPGR) with T_{acq} = 16 sec, interleaved with the periods of FSE acquisition with the number of averages of 1, 2, and 3 (Table II) for a total scan time of 4:37 min. Temperature maps were generated offline with proton resonance frequency shift (PRF) technique.

F. In vivo experiment

The study protocol was approved by the university's Institutional Animal Care and Use Committee. A catheter was placed into each common carotid artery of a single swine (43.2 kg, female), using a 30 cm × 30 cm flat panel C-arm X-ray system guidance (Cios Alpha, Siemens Healthineers, Munich, Germany). A gradient echo (GRE) sequence was acquired for visualization, and a Bloch-Siegert B_1+ map [20], [21] was acquired for flip angle quantification, using a sagittal scan plane, a 10 mm slice thickness, and the imaging parameters in Table II. The same scanner and coils were used as in the *in vitro* experiments, and either a coronal or sagittal scan plane was used, with a 10 mm slice thickness. An ROI was manually drawn around the entire marker to measure the mean signal, and then the ratio with the nearby background water signal was calculated to measure the relative amplification factor

III. Results

A. Resonant marker

The microscope images of the 10-turn helical trace are shown in different orientations, showing the double helix, the cross-over points, and the capacitor (Fig. 2b). The estimated maximal thickness is 2.264 mm due to an estimated 16 μm z-height thickness at the cross-over points, compared to approximately 3.2 mm maximal thickness for a hand-built resonant marker (Fig. 2c, d), including heat shrink.

B. In vitro image acquisition

The low flip angle bSSFP sequence (5° and 15°) shows the signal amplification of the markers relative to the background signal, in comparison with the high flip angle (90°) sequence (Fig. 3a). For the B_1+ map sequence, the relative amplification factor measured 1.67 in the parallel orientation, and in the perpendicular orientation, 1.63 (Fig. 3b). Two line plots of the bSSFP signal show the alternating signal between the helices (Fig. 3c).

C. Simulations

The magnetic flux density is shown for the double helix wireless resonant circuit and the surrounding region, showing patterns of enhancement and cancellation, and confirming the experimental results (Fig. 3d).

D. Temperature measurements

No appreciable heating was measured by the temperature probes (Fig. 4 a, b). MR thermometry images confirmed this by demonstrating no detectable heating (Fig. 4c).

E. In vivo experiment

The coronal GRE sequence shows good signal and contrast for the catheter on the left side (Fig. 5a), and the two catheter placements can be seen on X-ray (Fig. 5b, c). The Bloch-Siegert B_1+ map sequence demonstrates quantification of the flip angles (Fig. 5d). The mean scaled signal of the marker was 9.07°, and the mean scaled signal of the background tissue was 5.0°, for a relative amplification factor of 1.81. Using a lower flip angle of 5°

demonstrates the low background signal, and the signal amplification of the marker (Fig. 5e). As the flip angle increases to 20°, there is more signal in the surrounding tissue, and the contrast decreases (Fig. 5f). With a higher flip angle of 45°, there is over-flipping within the marker, causing a decreased signal, while the background tissue signal increases (Fig. 5g).

IV. DISCUSSION

We developed a fully printed and functional wireless resonant marker on a catheter for MRI tracking using aerosol jet deposition. A double helical inductor and a long capacitor were printed using silver nanoparticle ink and polyimide ink on a polymer catheter. The method consisted of a resonant circuit, in the form of a distributed LC circuit, which inductively coupled with the MR signal, as well as the RF receiver coils, to make the system wireless. Preliminary feasibility of using the marker in an interventional MRI setting was demonstrated *in vitro* and *in vivo*, and no appreciable heating was measured. This method introduces a complete, low profile resonant marker that is possible to print on a polymer catheter, and exhibits good tracking characteristics at 3T.

A resonant marker and catheter system of this size may allow further navigation into more distal vessels than prior approaches to endovascular interventional MRI allowed. The average internal carotid artery diameter is 4.66 ± 0.78 mm for women, and 5.11 ± 0.87 mm for men [23]. Given that our final PEEK catheter with the aerosol jet deposited circuits had an outer diameter of approximately 2.264 mm (6.78 Fr) and the hand-wound prototypes had an OD of approximately 3.2 mm (9.6 Fr), the aerosol jet-deposited catheter can more readily and safely navigate most cervical internal carotid arteries, which is the location where guide catheters generally terminate in the setting of contemporary bi-axial or tri-axial stroke treatments.

Other groups have used aerosol deposition to print the inductor of a resonant marker for MRI tracking. A prior group used aerosol deposition to print a gold plated copper solenoid inductor on a catheter, and connected it to a 100 pF discrete capacitor, with dimensions 1 mm × 0.5 mm × 0.6 mm, inside the catheter lumen [24], and electromagnetic simulations concurred with experimental validation at 1T [19]. Moving towards printing the marker entirely on the surface, another group demonstrated feasibility in depositing a single layer of a dielectric, lead zirconate titanate, at room temperature using aerosol deposition, in order to be compatible with the low melting temperature substrate of the polymer catheter, and measured the permittivity (ε) to be about 11 at 1 MHz [25]. The authors detected a resonant response at 43 MHz (1T) based on benchtop tests, but image enhancement for tracking purposes was not demonstrated [25]. We have extended these principles to demonstrate a working resonant marker prototype operating at 3T.

We discovered several trends during this study that provide insight into different design and microfabrication methods. The distributed capacitance of the long twin-lead transmission line allows the interventional radiologist to visualize the length and orientation of the catheter, which is similar to the tracking characteristics of some catheters tracking markers under X-ray. Similar wireless devices have been tracked using an interleaved sequence, where a low flip angle RF pulse, with phase-dithering applied, is followed by gradient-echo

readouts along the x, y, or z gradient axes, which is multiplexed with a Hadamard scheme [11]. The unique pattern at the tip of the catheter clearly delineates the tip, and pattern recognition could be used to determine the orientation and direction of the catheter. We experimentally observed different magnetic field zones, in the helical region, and the leaking flux region of the transmission line capacitor, generating unique field patterns. For the aerosol jet deposition printing, the total amount of time required was approximately 6–7 hours. A spray coating method to apply the top insulation layer was explored in order to save processing time; however, the coating showed uneven distribution of ink leading to ink pooling and fractures. We did not observe any image artifact from the polymer catheters themselves, and we anticipate minimal susceptibility-induced artifact, since PEEK has less than a 3 ppm difference in magnetic susceptibility from that of water and tissue [26].

This study considered printing markers on catheters that are manipulated by interventional radiologists; however, these techniques may be helpful for other MR applications. One group recently published a closed-loop method for controlling a rotational joint using robotics in combination with inductively coupled coils as fiducial markers [27]. Clinical applications may include printing these markers on catheters for MR-guided electrophysiology procedures in the large cardiac chambers [28]. A wireless resonant marker could also be incorporated onto an endovascular imaging coil, as has been demonstrated previously [29].

While the strengths of this work include the proof of concept of printing a complete LC circuit using aerosol deposition and a double helix inductor, this study does have limitations. The circuit design is limited by the significant length of the capacitor. Inductively coupled coils amplify the specific absorption rate (SAR) by coupling to both the electric and magnetic fields. It is possible that there are unwanted parasitic capacitance effects through the water phantom, due to the proximity of the circuit components near each other, and there are likely some common RF mode contributions due to the electric field coupling. A majority of signal appears to come from the capacitor, due to the displacement current. A dielectric ink with a higher permittivity could be used to shorten the capacitor. While one group explored the use of lead zirconate titanate as a dielectric with higher permittivity [25], our approach avoids the safety issues with using lead by keeping the cure temperature at a temperature just low enough (140°C) to avoid melting the outermost layer of catheter, since the thermoplastic elastomer has a melting temperature of 134–174°C. Different capacitor designs could also be used to reduce the overall electrical length, while keeping the capacitance the same. The skin depth of silver at 128 MHz should be 5.603 μm, and the conductive traces are estimated to have a total thickness of about 4 μm. Assuming similar values for the silver nanoparticle ink traces, the conductor thickness is thinner than the skin depth, and so with a thicker conductive path, the losses could be less, and the B_1+ amplification higher. Since the circuit was sealed with the polyimide ink, we did not measure the total equivalent resistance of the coil. Additionally, at each cross-over point of the double helix inductor, a capacitor is effectively formed, resulting in some self capacitance.

While we observed no obvious temperature increase in the temperature probe experiment and the MR thermometry experiment, the possibility remains that the local flip angle

amplification could result in heating and increased local SAR. The resonant marker was tested at the center of the magnet bore, but the highest electric fields, and therefore heating, are expected at the edge of the bore. Thorough safety analyses using the standard measurement for RF-induced heating, including both experiments and simulations, should be performed before any human studies [22].

There are several other possible solutions to mitigate RF-induced heating. One common hardware solution is to decouple the circuit during RF transmission by adding anti-parallel or crossed decoupling diodes to the circuit to limit the amplification [30]. These commercial diodes are currently available as thin wafers, which we will consider in the future. One group implemented optically detunable LC circuits [31], [32], using a laser diode to illuminate a photodiode through an optical fiber, in order to decouple the resonant marker. Another group recently demonstrated feasibility of an all-printed diode at ultra-high frequency, which could be printed with a similarly low profile as the resonant marker [33]. A software-based solution to potential heating could be to use a parallel transmission system and optimization approach to control RF induced heating [34]. An important safety consideration is transmit calibration, which may be heterogeneous throughout the volume.

The MRI experiments and post-processing also contain some limitations. The regions of interest drawn include a heterogeneous amount of signal due to the magnetic field pattern of the double helix, which may affect the relative signal amplification. *In vivo*, there are a variety of possible motion artifacts, due to respiration, cardiac, or pulsatile blood flow effects. We did not compensate for any of these effects, and in future experiments, motion compensation techniques, such as respiratory gating, may improve the signal amplification factor.

V. Conclusion

Imaging, B_1+ mapping, and temperature experiments demonstrated that the wireless resonant circuit printed on an endovascular guide catheter produces an induced current, transferring the RF into local signal amplification. We demonstrated proof-of-principle of microfabricating a fully aerosol jet-deposited complete LC circuit with a double helix inductor. The *in vivo* experiment at 3T further demonstrated that this method could potentially be used for a low profile guide catheter that can be tracked under MRI for endovascular neurointerventional applications.

Acknowledgment

The authors gratefully acknowledge Andrew Chu and Dave Barry at Penumbra, Inc., for in-kind provision of catheter materials, Steven Conolly, PhD and Lucas Carvajal for engineering discussions, Labonny Biswas, PhD and Graham Wright, PhD for discussions about real-time tracking, and Jay F. Yu, Galen Reed, PhD, and R. Reeve Ingle, PhD for assistance with RTHawk.

This work was supported in part by NIH Grants R01 EB012031, R01 CA194533, and R21 EB020283 as well as the National Center for Advancing Translational Sciences of the NIH under Award Number: UL1 TR001872 (UCSF-CTSI Catalyst Award) and TL1 TR001871 (Prescient Postdoctoral Fellowship). Its contents are solely the responsibility of the authors and do not necessarily represent the official views of the NIH.

References

[1]. Benjamin EJ et al., “Heart Disease and Stroke Statistics-2018 Update: A Report From the American Heart Association.,” Circulation, vol. 137, no. 12, pp. e67–e492, 3 2018. [PubMed: 29386200]

[2]. Rai AT et al., “A population-based incidence of acute large vessel occlusions and thrombectomy eligible patients indicates significant potential for growth of endovascular stroke therapy in the USA,” J. Neurointerv. Surg, vol. 9, no. 8, pp. 722–726, 8 2017. [PubMed: 27422968]

[3]. González RG, “Imaging-guided acute ischemic stroke therapy: From ‘time is brain’ to ‘physiology is brain’.,” AJNR. Am. J. Neuroradiol, vol. 27, no. 4, pp. 728–35, 4 2006. [PubMed: 16611754]

[4]. Nogueira RG et al., “Thrombectomy 6 to 24 Hours after Stroke with a Mismatch between Deficit and Infarct,” N. Engl. J. Med, vol. 378, no. 1, pp. 11–21, 1 2018. [PubMed: 29129157]

[5]. Albers GW et al., “Thrombectomy for Stroke at 6 to 16 Hours with Selection by Perfusion Imaging.,” N. Engl. J. Med, vol. 378, no. 8, pp. 708–718, 2 2018. [PubMed: 29364767]

[6]. Konings MK, Bartels LW, Smits HFM, and Bakker CJG, “Heating Around Intravascular Guidewires by Resonating RF Waves,” J. Magn. Reson. Imaging, vol. 12, no. 1, pp. 79–85, 7 2000. [PubMed: 10931567]

[7]. Yang JK et al., “Interventional magnetic resonance imaging guided carotid embolectomy using a novel resonant marker catheter: demonstration of preclinical feasibility.,” Biomed. Microdevices, vol. 19, no. 4, p. 88, 9 2017. [PubMed: 28948399]

[8]. Glowinski A, Kürsch J, Adam G, Bücker A, Noll TG, and Günther RW, “Device visualization for interventional MRI using local magnetic fields: basic theory and its application to catheter visualization.,” IEEE Trans. Med. Imaging, vol. 17, no. 5, pp. 786–93, 10 1998. [PubMed: 9874303]

[9]. Burl M, a Coutts G, and Young IR, “Tuned fiducial markers to identify body locations with minimal perturbation of tissue magnetization.,” Magn. Reson. Med, vol. 36, no. 3, pp. 491–3, 9 1996. [PubMed: 8875424]

[10]. Kaiser M et al., “Resonant marker design and fabrication techniques for device visualization during interventional magnetic resonance imaging,” Biomed. Eng. / Biomed. Tech, vol. 60, no. 2, 1 2015.

[11]. Rube MA, Holbrook AB, Cox BF, Houston JG, and Melzer A, “Wireless MR tracking of interventional devices using phase-field dithering and projection reconstruction.,” Magn. Reson. Imaging, vol. 32, no. 6, pp. 693–701, 7 2014. [PubMed: 24721007]

[12]. Celik H, Ulutürk A, Talı T, and Atalar E, “A catheter tracking method using reverse polarization for MR-guided interventions,” Magn. Reson. Med, vol. 58, no. 6, pp. 1224–1231, 12 2007. [PubMed: 18046701]

[13]. Quick HH et al., “Interventional magnetic resonance angiography with no strings attached: Wireless active catheter visualization,” Magn. Reson. Med, vol. 53, no. 2, pp. 446–455, 2005. [PubMed: 15678524]

[14]. Kuehne T, Fahrig R, and Butts K, “Pair of resonant fiducial markers for localization of endovascular catheters at all catheter orientations,” J. Magn. Reson. Imaging, vol. 17, no. 5, pp. 620–624, 2003. [PubMed: 12720274]

[15]. Ellersiek D et al., “A monolithically fabricated flexible resonant circuit for catheter tracking in magnetic resonance imaging☆,” Sensors Actuators B Chem, vol. 144, no. 2, pp. 432–436, 2 2010.

[16]. Thorne BR, Lillaney P, Losey AD, Zhang X, Pang Y, and Hetts SW, “Micro Resonant Marker for Endovascular Catheter Tracking in Interventional MRI: In Vitro Imaging at 3T,” in Proc. Intl. Soc. Mag. Reson. Med, 2014, vol. 21, no. 2013, p. 2327.

[17]. Thorne BRH, V Lillaney P, Losey AD, and Hetts SW, “Omnidirectional mri catheter resonator and related systems, methods, and devices,” WO2015164806A1, 2015.

[18]. Paulsen JA, Renn M, Christenson K, and Plourde R, “Printing conformal electronics on 3D structures with Aerosol Jet technology,” in 2012 Future of Instrumentation International Workshop (FIIW) Proceedings, 2012, pp. 1–4.

[19]. Krug J, Will K, and Rose G, “Simulation and experimental validation of resonant electric markers used for medical device tracking in magnetic resonance imaging.,” Conf. Proc. … Annu. Int. Conf. IEEE Eng. Med. Biol. Soc. IEEE Eng. Med. Biol. Soc. Annu. Conf, vol. 2010, pp. 1878–81, 8 2010.

[20]. Sacolick LI, Wiesinger F, Hancu I, and Vogel MW, “B1 mapping by Bloch-Siegert shift.,” Magn. Reson. Med, vol. 63, no. 5, pp. 1315–22, May 2010. [PubMed: 20432302]

[21]. Khalighi MM, Rutt BK, and Kerr AB, “RF pulse optimization for Bloch-Siegert B +1 mapping,” Magn. Reson. Med, vol. 68, no. 3, pp. 857–862, 9 2012. [PubMed: 22144397]

[22]. “ASTM F2182–11a, Standard Test Method for Measurement of Radio Frequency Induced Heating On or Near Passive Implants During Magnetic Resonance Imaging,” West Conshohocken, PA, 2011.

[23]. Krejza J et al., “Carotid Artery Diameter in Men and Women and the Relation to Body and Neck Size,” Stroke, vol. 37, no. 4, pp. 1103–1105, 4 2006. [PubMed: 16497983]

[24]. Will K et al., “Pre-tuned resonant marker for iMRI using aerosol deposition on polymer catheters,” in Society of Photo-Optical Instrumentation Engineers, 2010, p. 76251Z.

[25]. Schimpf S, Brose A, and Schmidt B, “Room Temperature Deposition of Lead Zirconate Titanate on Polymer as Part of a Magnetic Resonance Imaging Marker,” Int. J. Appl. Ceram. Technol, vol. 9, no. 1, pp. 67–73, 1 2012.

[26]. Schenck JF, “The role of magnetic susceptibility in magnetic resonance imaging: MRI magnetic compatibility of the first and second kinds.,” Med. Phys, vol. 23, no. 6, pp. 815–50, 6 1996. [PubMed: 8798169]

[27]. An J, Webb AG, Shah DJ, Chin K, and V Tsekos N, “Manipulator-driven selection of semi-active MR-visible markers,” Int. J. Med. Robot. Comput. Assist. Surg, vol. 14, no. 1, p. e1846, 2 2018.

[28]. Hilbert S et al., “Real-time magnetic resonance-guided ablation of typical right atrial flutter using a combination of active catheter tracking and passive catheter visualization in man: initial results from a consecutive patient series.,” Europace, vol. 18, no. 4, pp. 572–7, 4 2016. [PubMed: 26316146]

[29]. Venkateswaran M et al., “Modeling Endovascular MRI Coil Coupling With Transmit RF Excitation,” IEEE Trans. Biomed. Eng, vol. 64, no. 1, pp. 70–77, 1 2017. [PubMed: 26960218]

[30]. Ooi MB, Aksoy M, Maclaren J, Watkins RD, and Bammer R, “Prospective motion correction using inductively coupled wireless RF coils.,” Magn. Reson. Med, vol. 70, no. 3, pp. 639–47, 9 2013. [PubMed: 23813444]

[31]. Wong EY, Zhang Q, Duerk JL, Lewin JS, and Wendt M, “An optical system for wireless detuning of parallel resonant circuits.,” J. Magn. Reson. Imaging, vol. 12, no. 4, pp. 632–8, 10 2000. [PubMed: 11042647]

[32]. Weiss S et al., “In vivo safe catheter visualization and slice tracking using an optically detunable resonant marker,” Magn. Reson. Med, vol. 52, no. 4, pp. 860–868, 10 2004. [PubMed: 15389956]

[33]. Sani N et al., “All-printed diode operating at 1.6 GHz.,” Proc. Natl. Acad. Sci. U. S. A, vol. 111, no. 33, pp. 11943–8, 8 2014. [PubMed: 25002504]

[34]. Gudino N et al., “Parallel transmit excitation at 1.5 T based on the minimization of a driving function for device heating,” Med. Phys, vol. 42, no. 1, pp. 359–371, 12 2014.

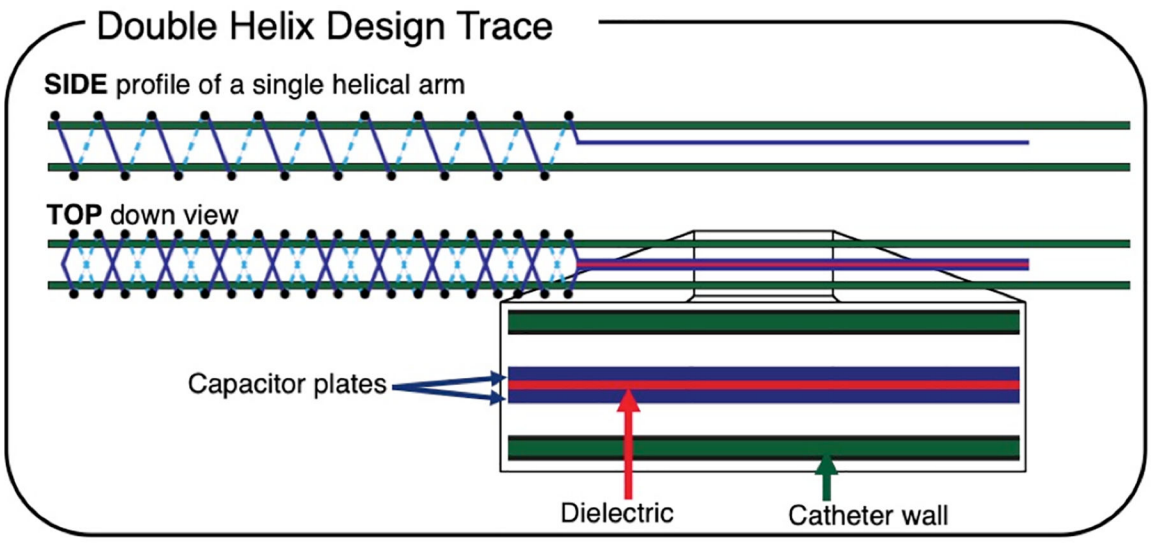

Fig. 1.

Schematic of the resonant marker design: an inductively coupled RF coil marker can be used for tracking during MRI. The side profile of a single helical arm is shown, as a single arm was printed first. The top-down view of the 10-turn double helix geometry of the inductor, along with the twin-lead transmission line capacitor, is shown with dielectric ink (red) and conductive ink (blue) traces. Solid lines indicate traces in front of the catheter, and dashed lines indicate traces behind the catheter (green).

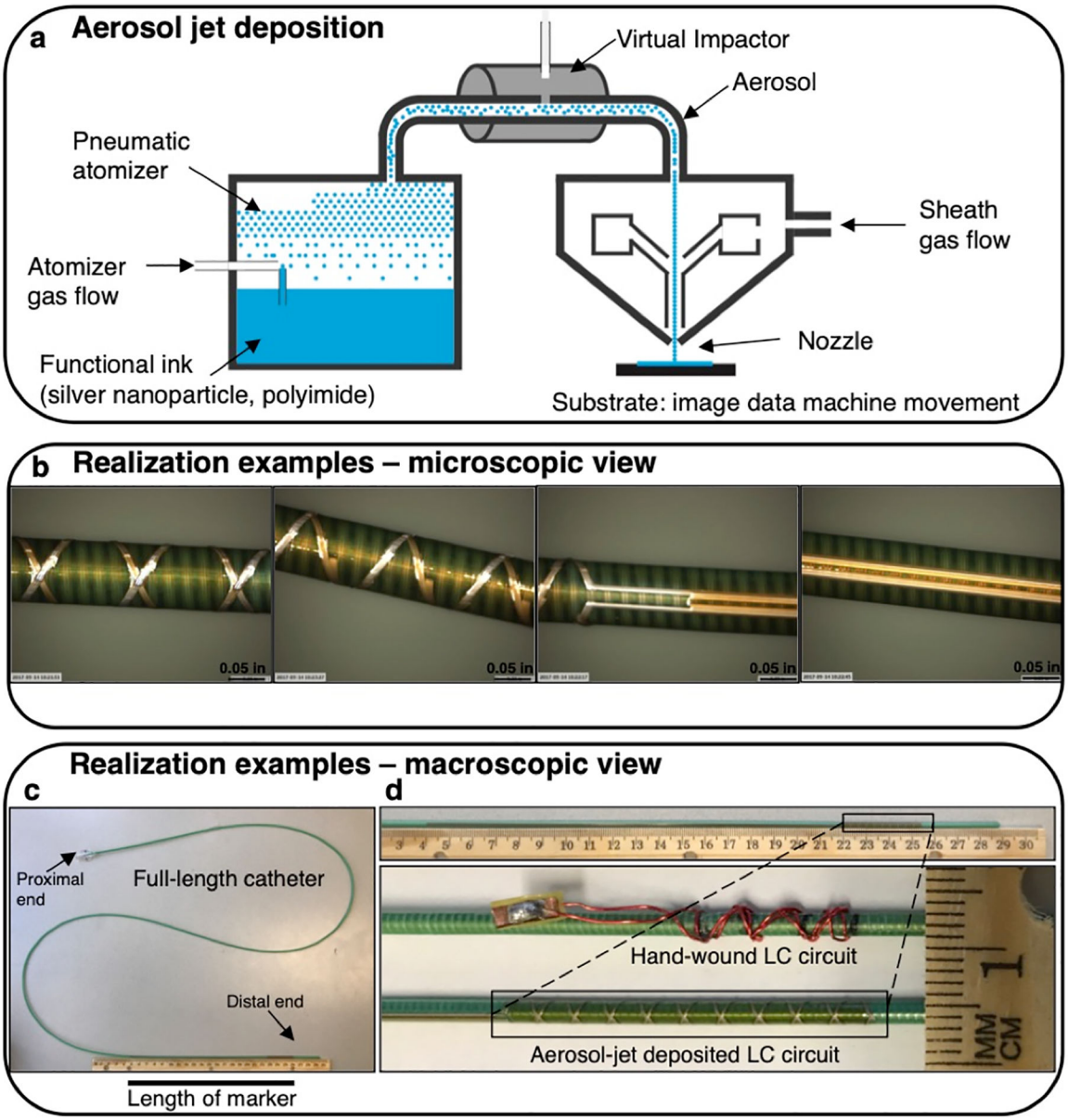

Fig. 2.

Fabrication method and realization example of aerosol jet deposited circuits. a) A simplified schematic of aerosol jet deposition is shown. Nitrogen gas is used for pneumatic aerosolization and propulsion with excess gas being stripped off by a virtual impactor and outer sheath gas collimates the beam and keeps the aerosol from contacting the nozzle. b) An example of a test printing process is shown. c) A realization example of the 10-turn double helix prints are shown. d) This marker print is shown in comparison with a hand-wound marker, demonstrating its extremely low profile.

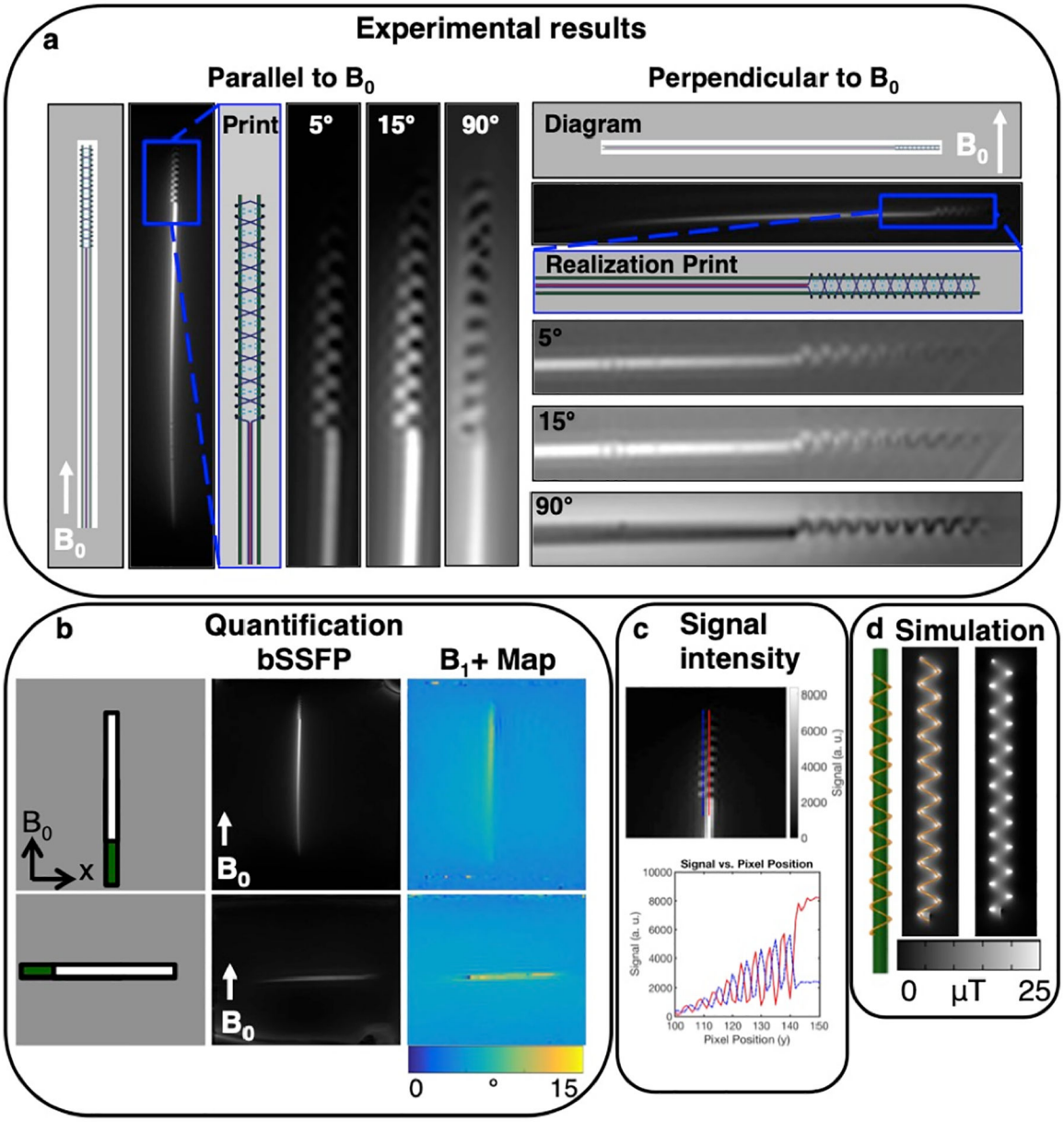

Fig. 3.

In vitro results in phantoms at 3T show good signal. The diagram, aerosol jet deposition prints, and bSSFP sequences of the double helix resonant marker are shown oriented a) parallel to and perpendicular to B_0 using a coronal scan plane, and a bSSFP sequence with a 10 mm slice thickness. The sequences with low flip angles of 5° and 15° show the surrounding signal amplification of the circuits, which can be compared with a 90° flip angle, showing the background and over-flipping of the signal. b) The bSSFP sequence, and B_1+ map are shown for the full-length marker. c) A line plot of the signal shows the alternating signal between the helices. d) Simulation of the electromagnetic fields confirms the magnetic field pattern.

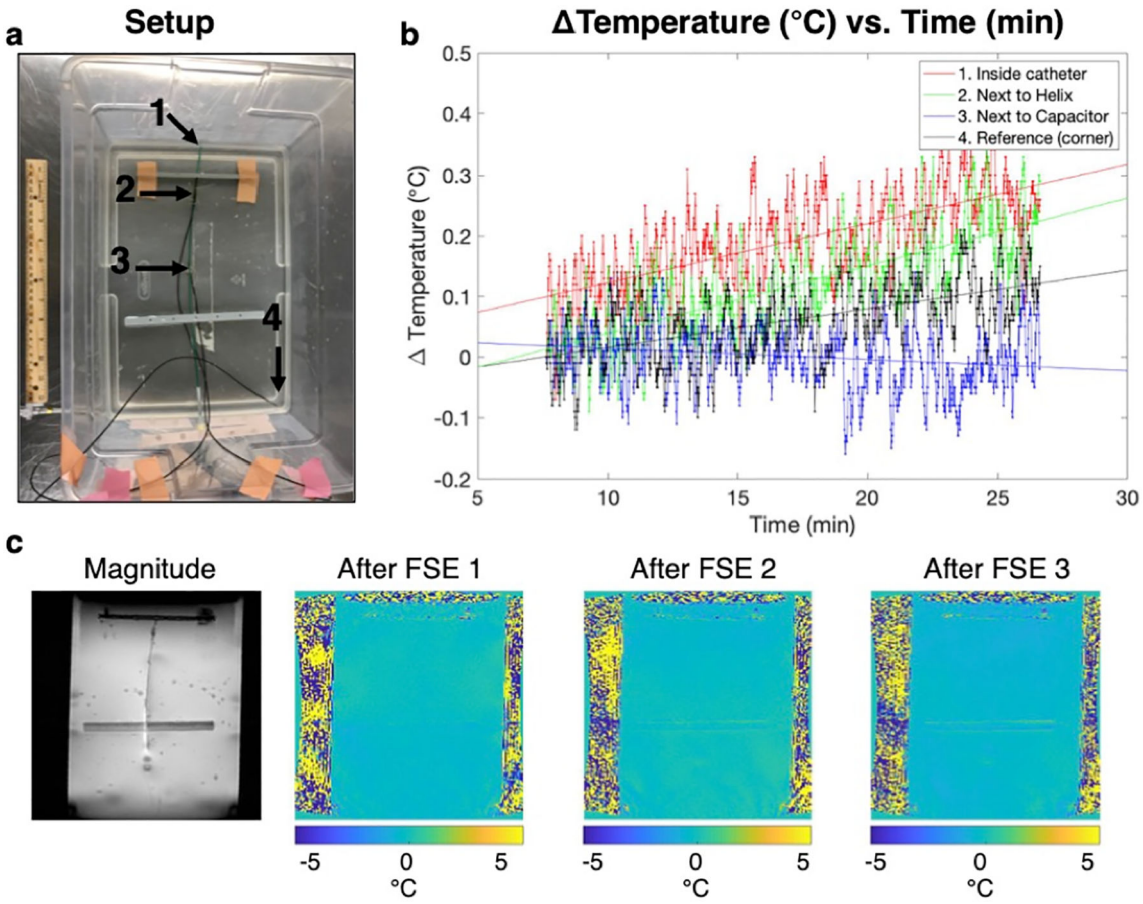

Fig. 4.

Temperature measurements and MR thermometry in a phantom at 3T demonstrate minimal heating. a) The setup of the temperature probes in the gel is shown. b) Compared to the reference probe, no substantial heating was observed. c) This was confirmed by MR thermometry maps after three FSE sequences, increasing in time.

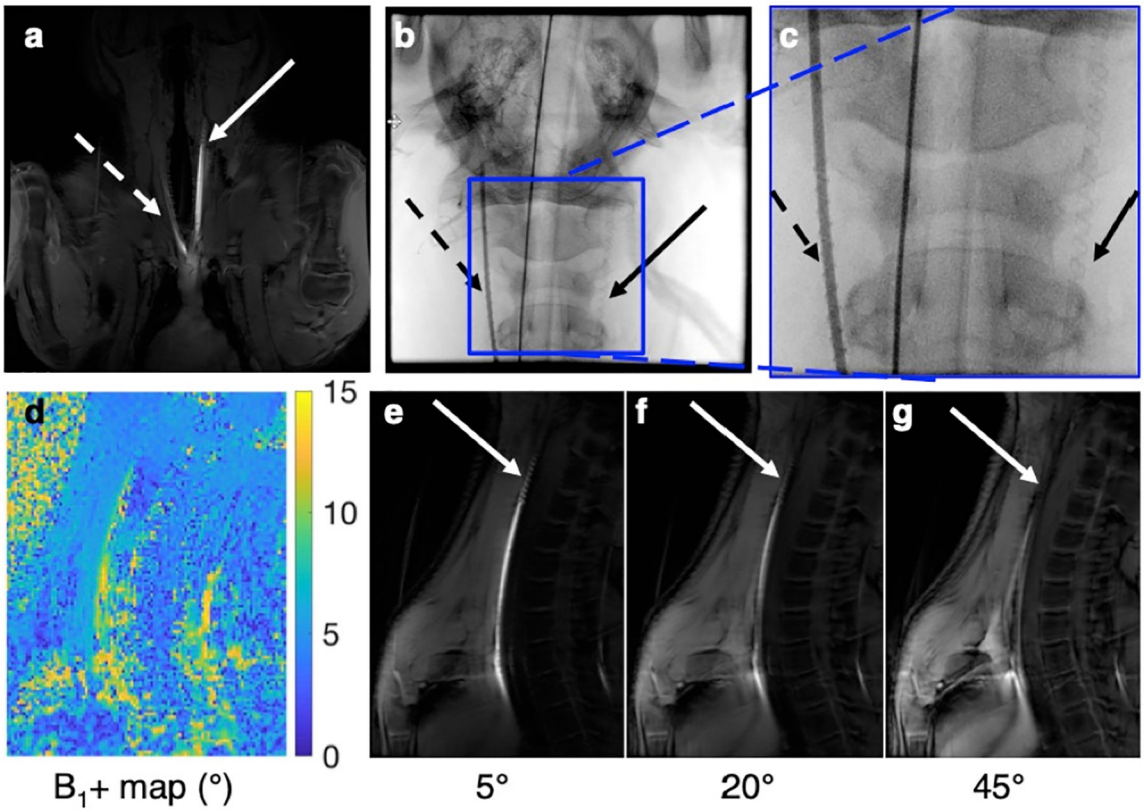

Fig. 5.

The wireless resonant markers demonstrate good signal in an *in vivo* preclinical scenario at 3T. The markers placed in the right (dashed arrow) and left (solid arrow) carotid arteries of a single swine are shown in a coronal scan plane under a) MRI and b) X-ray, which are more easily seen under c) magnification (left artery with contrast, and the right artery without contrast). d) In a sagittal plane, the B_1+ map quantifies signal amplification. e) The GRE sequence with a lower flip angle (5°) demonstrates low background signal and marker signal amplification. f) As the flip angle increases (20°), there is more signal in the surrounding tissue. g) With a higher flip angle (45°), there is over-flipping near the marker, causing a decreased signal, while the background signal increases.

TABLE I

DIMENSIONS OF THE POLYMER CATHETER AND THE MATERIAL PROPERTIES OF THE INKS ARE REPORTED FOR THE AEROSOL JET-DEPOSITED MARKERS

Material	Dimensions
Catheter	
Inner diameter of Polytetrafluoroethylene (PTFE) liner	1.770–1.783 mm
PTFE liner wall thickness	0.019–0.025 mm
Polyether ether ketone (PEEK) fiber diameter	0.127 mm
Polyether block amide wall thickness (Pebax® 72D)	0.076 mm
Catheter outer diameter	2.248 mm (6.75 Fr)
Overall catheter length	140 cm
Silver nano-flake ink (NovaCentrix HPS 108AE1)	
Particle Size	400–700 nm
Solid content	60% wt
Sintering condition	60 mins or longer at ≥120°C
Resistivity	484 μΩ-cm (140°C cure temp)
Printing Nozzle diameter	200 μm
Polyimide ink (Sigma Aldrich)	
Solid content	11%
Sintering Condition	30 minutes between steps at ≥120°C, 2 hours for final cure
Dieletric Constant	3.6–3.7
Printing Nozzle diameter	300 μm

TABLE II

MRI Acquisition Parameters for the Datasets in this Study

Sequence	TE (MS)	TR (MS)	FA (°)	BW (KHZ)	FOV (CM^2)	MATRIX SIZE
In vitro						
bSSFP	1.7	4.63	5/15/90	125	30, 36	384×384
B_1+ map	13.4	28	5	15.63	36	128×128
Temperature						
GRE	3.7	100	5/20/45	15.63	24, 30	384×384
Thermometry						
fSPGR	16.1	120	30	7.81	32	160×128
FSE	14	425	90/180	15.63	32	256×256
In vivo						
GRE	3.7	100	5/20/45	15.63	24, 30	384×384
B_1+ map	13.2	28	5	15.63	24	128×128